Chaos, Solitons and Fractals 151 (2021) 111270

Contents lists available at ScienceDirect

Chaos, Solitons and Fractals

Nonlinear Science, and Nonequilibrium and Complex Phenomena

journal homepage: www.elsevier.com/locate/chaos

Stochastic variability of regular and chaotic dynamics in 2D metapopulation model

Alexander Belyaev, Irina Bashkirtseva, Lev Ryashko*

Department of Theoretical and Mathematical Physics, Ural Federal University, Lenina, 51, Ekaterinburg, 620000, Russian Federation

ARTICLE INFO

Article history:
Received 12 June 2021
Accepted 23 June 2021
Available online 30 July 2021

Keywords:
Metapopulation
Random disturbances
Riddled basins
Stochastic sensitivity
Order-chaos transitions

ABSTRACT

A behavior of metapopulation consisting of two coupled subsystems modeled by the Ricker map is considered. We study how dynamics of the metapopulation changes under increase in the intensity of migration between subpopulations. For the deterministic model, a variety of equilibrium, periodic, quasiperiodic, and chaotic attractors is described. An impact of random disturbances on the behavior of metapopulation is studied both numerically and analytically with the help of confidence domains. A phenomenon of the noise-induced temporal stabilization of the unstable equilibrium is discovered. We point out the special role of transients and fractal riddled basins in the noise-induced transitions from order to chaos.

1. Introduction

At present, in mathematical modeling, research interest is directed towards complex phenomena observed in coupled systems. Being coupled, even simple dynamical systems can be quite intricate, demonstrating a rich variety of qualitatively different regimes, both regular and chaotic [1–3].

Mathematical studies of underlying reasons of coupling-induced phenomena are motivated by applications to ecology [4], epidemiology [5], brain activity [6], engineering [7], social networks [8], etc. Based on the modern theory of bifurcations, the analysis of complex processes in coupled systems reveals such nonlinear phenomena as transitions between order and chaos, crisis-induced intermittency, transverse instability and riddled basins, birth of multi-layered tori (see e.g. [9–14]). The presence of stochastic fluctuations gives additional variety to possible dynamical modes in coupled systems and complicate their analysis [15–21].

Population dynamics is one of the most important fields of science where effects of coupling are naturally present. Dynamics of metapopulations attracts attention of many researchers, both biologists and mathematicians [22–24]. Studies of the effects of mutual migrations in metapopulations are of a special interest [25–30].

In the present paper, we examine the spatially structured metapopulation consisting of two coupled subsystems with local dynamics defined by the Ricker map [31]. In isolated subsystems, various modes can be observed: equilibrium, periodic, and chaotic. In this paper, we focus on the case when isolated units exhibit equilibrium regimes. The aim of the study is to analyze the diversity of modes of collective dynamics with a change in the intensity of coupling and random noise.

2. Deterministic model

Consider a system of two coupled population units modeled by the Ricker map [31] with the function $f(x) = x\exp(\mu(1-x))$

$$\begin{aligned} x_{t+1} &= f(x_t) + \eta_t, \\ y_{t+1} &= f(y_t) - \eta_t. \end{aligned} \tag{1}$$

Here, x_t, y_t are densities of subpopulations, and η_t characterizes mutual flows between them. For $\eta_t \equiv 0$, subsystems are independent of each other, and its dynamics is determined by the parameter μ of intrinsic growth rate. Regimes of dynamics of the isolated Ricker model $x_{t+1} = x_t\exp(\mu(1-x_t))$ under variation of μ are presented by the bifurcation diagram in Fig. 1. For any μ, this isolated model exhibits the equilibrium $\bar{x} = 1$ that is stable for $0 < \mu < 2$. At $\mu = 2$, this equilibrium becomes unstable and for increasing μ, a well-known Feigenbaum tree with regular and chaotic attractors is observed.

It is assumed that populations inhabit adjacent territories, so migration of individuals between these territories is possible. To model the migration η_t, we will use the following law:

$$\eta_t = \sigma(y_t - x_t). \tag{2}$$

So, migration between subpopulations is proportional to the difference between y_t and x_t with the coupling coefficient σ. The parameter σ regulates a strength of the migration flow. To provide non-negativeness of x_t and y_t in dynamics of the system (1), (2), we use the appropriate truncation.

* Corresponding author.
E-mail address: Lev.Ryashko@urfu.ru (L. Ryashko).

https://doi.org/10.1016/j.chaos.2021.111270
0960-0779/

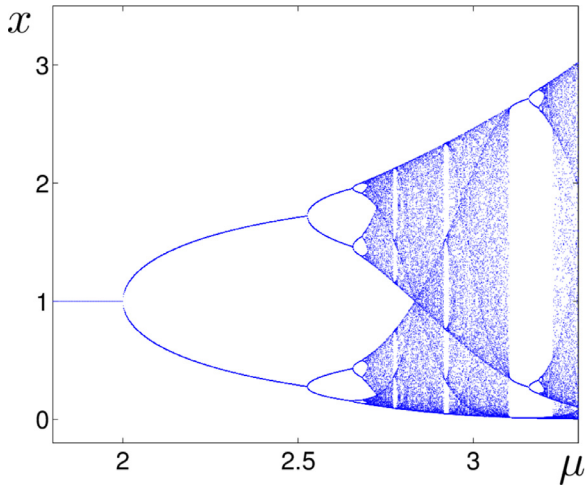

Fig. 1. Bifurcation diagram of the isolated Ricker model.

In the present paper, we focus on the study of effects of mutual flows for the case when isolated subpopulations are in the same stable equilibrium mode. Here and further, we fix the value $\mu = 1.8$ and investigate how variation of the migration intensity σ changes a common dynamics of the metapopulation (1), (2).

Note, that the system (1), (2) for any σ has the equilibrium (1,1) which is stable for $\sigma < 0.1$. Changes in dynamical behavior of the system (1), (2) versus parameter σ are described by the bifurcation diagram in Fig. 2. Here, along with x-coordinates of attractors (blue), the largest Lyapunov exponent Λ is shown by red.

As can be seen, under increasing σ, the equilibrium loses its stability at $\sigma = 0.1$ and the stable 2-cycle appears. This 2-cycle transforms into a two-torus, further two-torus is replaced by a discrete cycle, and finally chaotic regime is observed. The largest Lyapunov exponent has zero values at bifurcation points, and positive values when the system (1), (2) is chaotic.

A variety of attractors of the system (1), (2) is illustrated in Fig. 3. Here, we show the equilibrium (1,1) for $\sigma = 0.08$, 2-cycle for $\sigma = 0.26$, two-torus for $\sigma = 0.298$, 22-cycle for $\sigma = 0.33$, 12-cycle for $\sigma = 0.42$ and various chaotic attractors for $\sigma = 0.353$, $\sigma = 0.362$, $\sigma = 0.366$, and $\sigma = 0.413$.

Different types of anti-phase oscillations appear in the system (1), (2): periodic, quasiperiodic, and chaotic. Some examples of these oscillating modes are shown in Fig. 4 where time series for the x, y-coordinates of solutions are plotted in blue and red, accordingly. In Fig. 4a for $\sigma = 0.26$ one can see how initial in-phase oscillations after short transient switch to anti-phase two-periodic synchronized mode. In Fig. 4b for $\sigma = 0.298$ anti-phase oscillations have quasiperiodic form. More complex forms of oscillations in chaotic mode are shown in Fig. 4c,d,e. Here, burst-type oscillations with alternation of in-phase and anti-phase fragments are clearly seen. A behavior of the system (1), (2) in the order window (see Fig. 2 right) is illustrated in Fig. 4f for $\sigma = 0.42$ where metapopulation exhibits anti-phase synchronization in 12-periodic form.

Thus, the behavior of the metapopulation modeled by the system (1),(2) is rather complex even in the simplest case when isolated subpopulations are in the same equilibrium mode. As one can see, migration can essentially change dynamics and cause both regular (periodic or quasiperiodic) and chaotic oscillatory regimes in the metapopulation. In the following Section, we will show how inevitable random disturbances in the parameter of the migration intensity impact the dynamics of metapopulation.

3. Stochastic model

Let us consider the system (1), (2) with the random disturbances in the coupling parameter σ:

$$\begin{aligned} x_{t+1} &= f(x_t) + (\sigma + \varepsilon\xi_t)(y_t - x_t), \\ y_{t+1} &= f(y_t) - (\sigma + \varepsilon\xi_t)(y_t - x_t). \end{aligned} \tag{3}$$

Here, ξ_t is uncorrelated Gaussian noise ε with parameters $\mathrm{E}\xi_t = 0$, $\mathrm{E}\xi_t^2 = 1$ and the noise intensity ε.

In the present study, we focus on the analysis of impact of such stochastic disturbances on the periodic oscillatory regimes.

3.1. How noise impacts 2-cycle

First, consider the stochastic system (3) with $\sigma = 0.26$ where for $\varepsilon = 0$ the deterministic attractor is 2-cycle (see red dots in Fig. 3a and time series in Fig. 4a).

In Fig. 5a,b, random states (green) of the stochastic system (3) and deterministic 2-cycle (red) are plotted for $\sigma = 0.26$ and two values of noise intensity, $\varepsilon = 0.01$ and $\varepsilon = 0.1$. As one can see, with increase in noise, the dispersion of random states around the deterministic attractor grows.

In Fig. 5c,d, corresponding time series are shown. For $\varepsilon = 0.01$, the system exhibits noisy anti-phase oscillations while noise with intensity $\varepsilon = 0.1$ causes temporal destruction of anti-phase synchronization.

With the further increase of noise intensity, a new stochastic phenomenon is observed. In Fig. 6, time series of the system (3) solutions are shown for $\varepsilon = 0.01$, $\varepsilon = 0.5$, and $\varepsilon = 1$. In Fig. 6a for $\varepsilon = 0.01$, one can see noisy oscillations around states of 2-cycle. For larger noise ($\varepsilon = 0.5$), after some transient, the amplitude of random states abruptly decreases and solutions begin to localize near the unstable equilibrium $(1, 1)$ (see Fig. 6b). Such a localization is temporal: one can see alternation of zones of stabilization and large-amplitude oscillations. So, the phenomenon of noise-induced temporal stabilization of the unstable equilibrium is

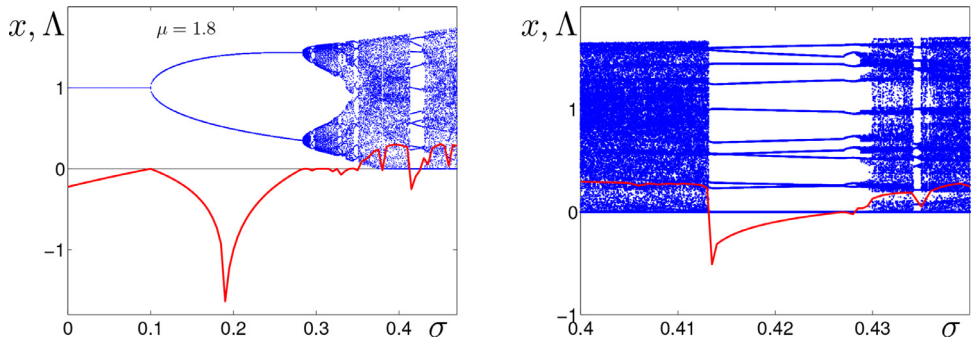

Fig. 2. Bifurcation diagram of the metapopulation system (1),(2) with $\mu = 1.8$.

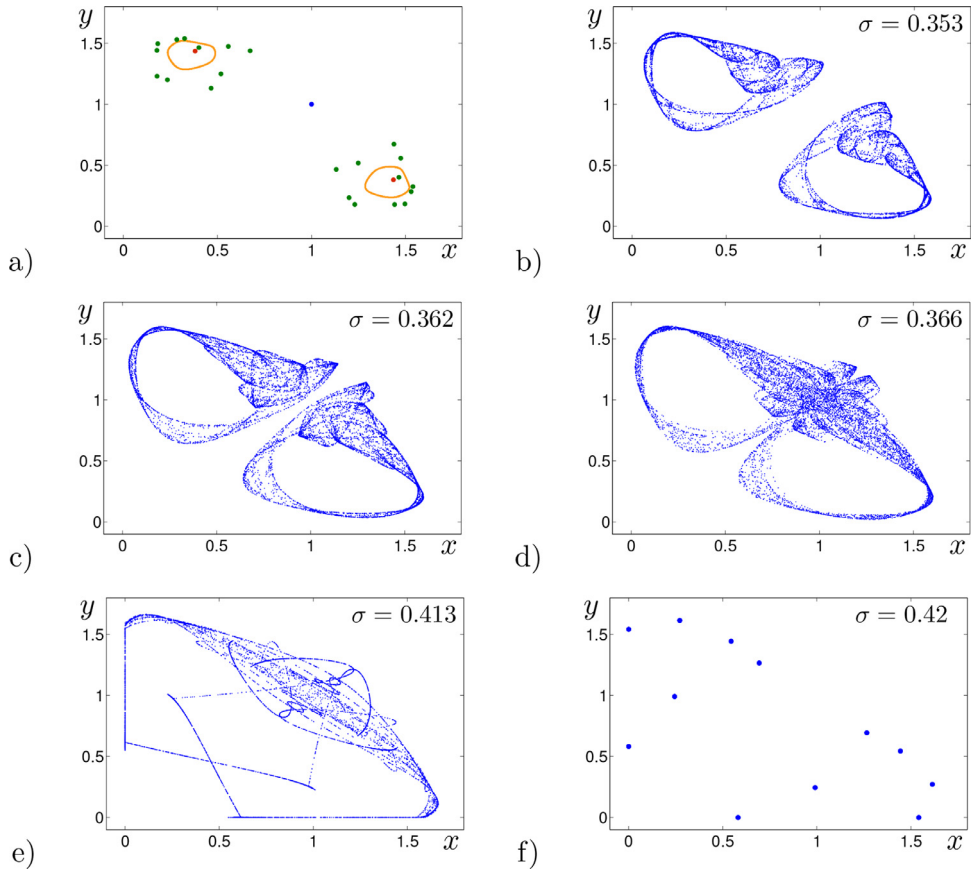

Fig. 3. Attractors of the metapopulation system (1),(2) with μ = 1.8: a) the equilibrium (1,1) for $\sigma = 0.08$ (blue), 2-cycle for $\sigma = 0.26$ (red), two-torus for $\sigma = 0.298$ (orange) and 22-cycle for $\sigma = 0.33$ (green); two-piece chaos for b) $\sigma = 0.353$ and c) $\sigma = 0.362$; one-piece chaos for d) $\sigma = 0.366$ and e) $\sigma = 0.413$; f) 12-cycle for $\sigma = 0.42$. (For interpretation of the references to color in this figure legend, the reader is referred to the web version of this article.)

observed. With the further increase of noise intensity (see Fig. 6c for $\varepsilon = 1$), the duration of the stabilization sections is reduced.

Results of the statistical analysis of this stochastic phenomenon are shown in Fig. 7 in detail. Here, we present the σ-zone where the system (1), (2) possesses 2-cycles as attractors. Figure 7a shows plots of the mean square deviation D of the random states of the stochastic system (3) from the unstable deterministic equilibrium (1,1) versus noise intensity for four values of the coupling parameter: $\sigma = 0.11$ (blue), $\sigma = 0.16$ (red), $\sigma = 0.2$ (green), and $\sigma = 0.26$ (orange). Here, one can see a general law: under increasing noise intensity, ε-zone in which the deviation is close to zero appears. This indicates the noise-induced localization of random states near the unstable equilibrium (1,1). As can be seen in Fig. 7a, after ε-zone of stabilization, the function D begins to grow.

Figure 7 b shows plots of the probability p of the residence of random states of the stochastic system (3) in the small circle $(x-1)^2 + (y-1)^2 \le 10^{-8}$ with the unstable equilibrium (1,1) as a center. As can be seen, and from the point of view of the probability distribution, the ε-zone where the noise stabilizes the system is rather narrow.

3.2. How noise impacts 22-cycle

Consider how noise impacts the system (1), (2) with $\sigma = 0.33$. In the deterministic case ($\varepsilon = 0$), for $\sigma = 0.33$, the system exhibits regular oscillatory regime with 22-cycle as attractor. States of this cycle are shown in Fig. 8a along with x, y-time series. As can be seen, oscillations of densities in sub-populations occur in anti-phase regime.

With increasing intensity of noise, two stages can be determined in the change of the behavior of the metapopulation. These stages are seen in Fig. 8b where random states and corresponding y-time series are shown for three values of the noise intensity.

For weak noise, random solutions slightly oscillate near the deterministic 22-cycle (see blue points for $\varepsilon = 0.0003$ in Fig. 8b). Under increasing noise, the first stage of the qualitative stochastic deformation of the system dynamics begins: the system transits to the more complicated regime of noisy 2-torus (see red points for $\varepsilon = 0.005$ in Fig. 8b). With further increase of noise, the third stage occurs: separate parts of this 2-torus merge because of stochastic mixing of random states, and the joint probabilistic distribution is formed (see green points for $\varepsilon = 0.05$ in Fig. 8b).

These stochastic transformations are accompanied by changes in values of the Lyapunov exponent $\Lambda(\varepsilon)$ shown in Fig. 8c. The function $\Lambda(\varepsilon)$ monotonously increases and becomes positive. This means that system dynamics transforms from regular to chaotic already at the first stage of stochastic deformation.

3.3. How noise impacts 12-cycle

Consider now a parameter zone near the bifurcation value $\sigma_{cr} = 0.413163$. As can be seen in bifurcation diagram (Fig. 2, right), as σ passes σ_{cr} from left to right, the deterministic system undergoes crisis bifurcation with the sharp transformation of chaotic attractor into the regular 12-cycle.

Examples of such attractors near the crisis bifurcation σ_{cr} are shown in Fig. 9. We will study the effect of noise on attractors in the order window located to the right of the point σ_{cr} using as

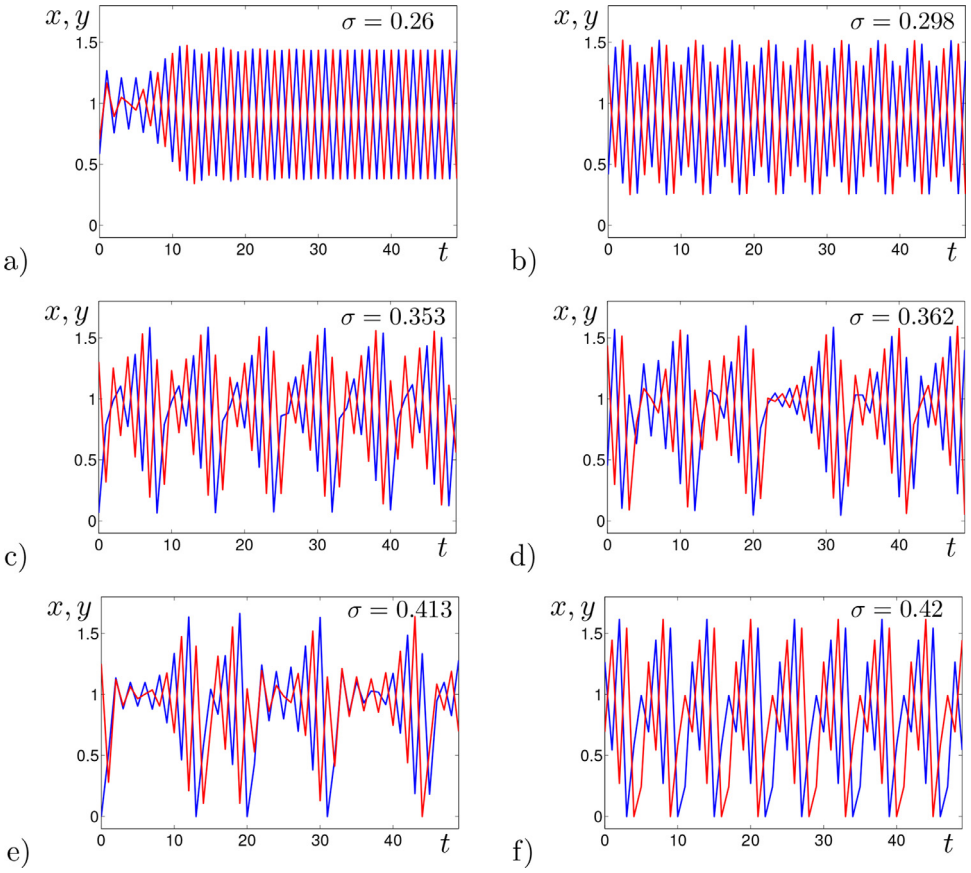

Fig. 4. Oscillatory modes of system (1), (2).

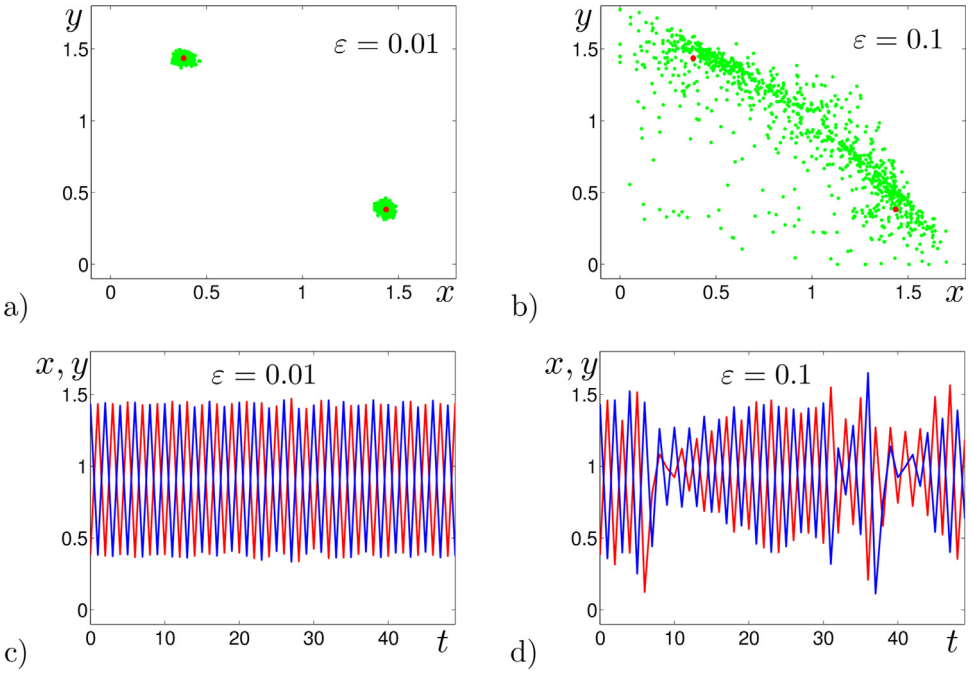

Fig. 5. Random states (green) of the stochastic system (3) with $\sigma = 0.26$ a) for $\varepsilon = 0.01$; b) for $\varepsilon = 0.1$. Points of the deterministic 2-cycle are shown by red. In c), d), corresponding time series are shown. (For interpretation of the references to color in this figure legend, the reader is referred to the web version of this article.)

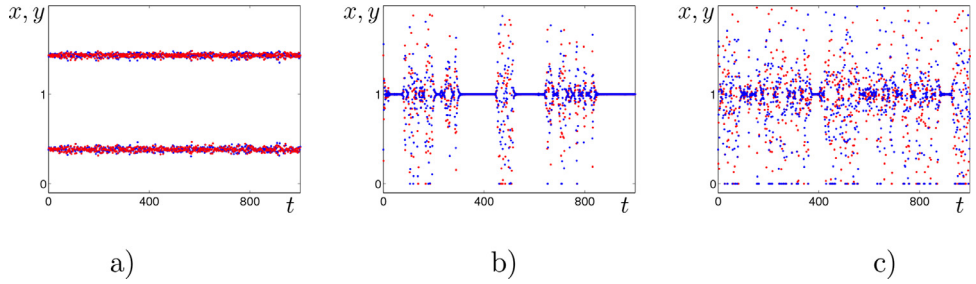

Fig. 6. Time series of x- and y-coordinates of solutions of the stochastic system (3) with $\sigma = 0.26$ for a) $\varepsilon = 0.01$, b) $\varepsilon = 0.5$, c) $\varepsilon = 1$.

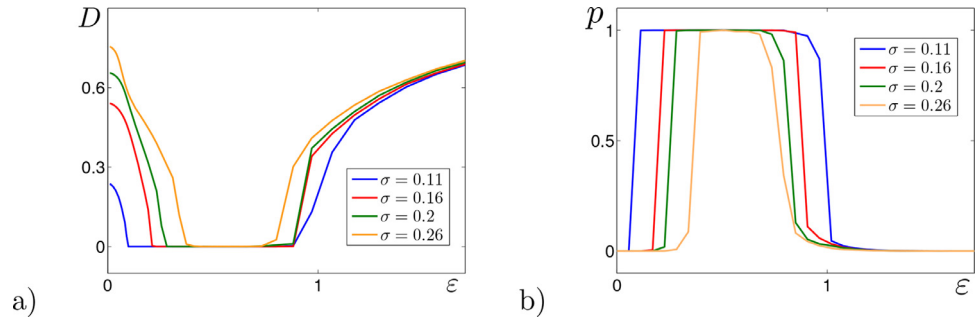

Fig. 7. Noise-induced temporal stabilization of the equilibrium (1,1): a) mean-square deviation D of random states of the system (3) from the equilibrium (1,1) for $\sigma = 0.11$ (blue), $\sigma = 0.16$ (red), $\sigma = 0.2$ (green), and $\sigma = 0.26$ (orange); b) probability of the residence of random states in the circle $(x-1)^2 + (y-1)^2 \le 10^{-8}$ for the same set of σ. (For interpretation of the references to color in this figure legend, the reader is referred to the web version of this article.)

a key example the 12-cycle observed for $\sigma = 0.42$. States of this deterministic cycle are shown by blue points in Fig. 10.

For weak noise, random states are localized near the deterministic cycle (see green points for $\varepsilon = 0.003$ in Fig. 10a).

Under increasing noise, sharp qualitative change in the probabilistic spatial distribution of random states occurs. This distribution is shown by green in Fig. 10b for $\varepsilon = 0.02$. As can be seen, the spatial location of random states looks similar to the deterministic chaotic attractor shown in Fig. 9 for $\sigma = 0.41316$.

Background of this stochastic phenomenon is related to the peculiarities of transient processes in the original deterministic model. Indeed, a type of the convergence to the attractor (12-cycle in considered case) significantly depends on the initial state. This is illustrated in the Fig. 11 for $\sigma = 0.42$. Here, by blue dot, the point $\bar{x} = 0.27138$, $\bar{y} = 1.61401$ of the stable deterministic 12-cycle is shown. Each state of this cycle becomes a stable equilibrium in the system (1), (2) in 12 steps. In Fig. 11 by green color we show basin of attraction of $(\bar{x}, \bar{y})$ in this system in 12 steps. As can be seen, this basin contains the solid subdomain $\mathcal{A}$. The complement $\mathcal{B}$ has a fractal riddled-like structure [10,32].

These two domains $\mathcal{A}$ and $\mathcal{B}$ allow us to separate two types of transients processes. Indeed, for initial data from the zone $\mathcal{A}$, solutions of the system (1), (2) in 12 steps quickly tend to the equilibrium $(\bar{x}, \bar{y})$. This is illustrated in Fig. 12 where states of the ensemble of solutions of the deterministic system starting at $t = 0$ from the nodes of the uniform grid on the red square $[0.23, 0.25] \times [1.57, 1.585] \subset \mathcal{A}$ are plotted. This red square is shown in the Fig. 11.

It should be noted that another type of the transient process for solutions starting in $\mathcal{B}$ is observed. In Fig. 13, states of the ensemble of system solutions starting at $t = 0$ from the nodes of the uniform grid on the blue square $[0.25, 0.27] \times [1.54, 1.555] \subset \mathcal{B}$ are plotted. In this transient process, metastable distribution similar to the chaotic attractor (Fig. 9) appears.

So, the domain $\mathcal{A}$ can be associated with a zone of regular dynamics in contrast with the domain $\mathcal{B}$ where chaotic transients are observed. Such a dichotomy of deterministic behavior allows one to explain the phenomenon of the stochastic generation of random distributions of the complex spatial form as in Fig. 10. The transition from the noisy 12-cycle (Fig. 10a) to the complex spatial distribution (Fig. 10b) can be analysed by the method of confidence domains.

The method of confidence domains allows us to approximate the spatial dispersion of random solutions around the deterministic attractor. In this approximation, stochastic sensitivity of the attractor to random disturbances is a key point. The stochastic sensitivity technique for regular (equilibria, cycles, tori) and chaotic attractors was elaborated in [33–35]. The method of confidence domains (ellipses, ellipsoids, bands, tori) was effectively used for the analysis of various stochastic phenomena in nonlinear systems [36–39].

In Fig. 11, confidence ellipses around $(\bar{x}, \bar{y})$ are plotted for $\varepsilon = 0.003$ and $\varepsilon = 0.02$. The smaller ellipse totally belongs to the domain $\mathcal{A}$ while the larger ellipse partially occupies the domain $\mathcal{B}$. This arrangement signals that for $\varepsilon = 0.003$ the stochastic system will exhibit noisy 12-cycle with small deviations from its deterministic states whereas for $\varepsilon = 0.02$ the new stochastic attractor with the complex spatial form will be generated. This analytical prediction is in a good agreement with results of the direct numerical simulation.

Let us consider how this stochastic transformation of the probabilistic distribution is related to the change of the largest Lyapunov exponent Λ. In Fig. 14, the plot of the $\Lambda(\varepsilon)$ is shown in red for the considered case $\sigma = 0.42$. As can be seen, with the increase of noise intensity, $\Lambda(\varepsilon)$ grows and changes its sign from minus to plus. Note that $\Lambda(0.003)$ is negative whereas $\Lambda(0.02)$ is positive. It means that for $\varepsilon = 0.003$ the stochastic attractor is regular but for $\varepsilon = 0.02$ the system dynamics is chaotic. The noise-induced transition from order to chaos can be seen in Fig. 14 for other values of σ. As one can see, the closer σ to the crisis bifurcation border $\sigma_{cr} = 0.413163$ the smaller noise causes the transition from order to chaos.

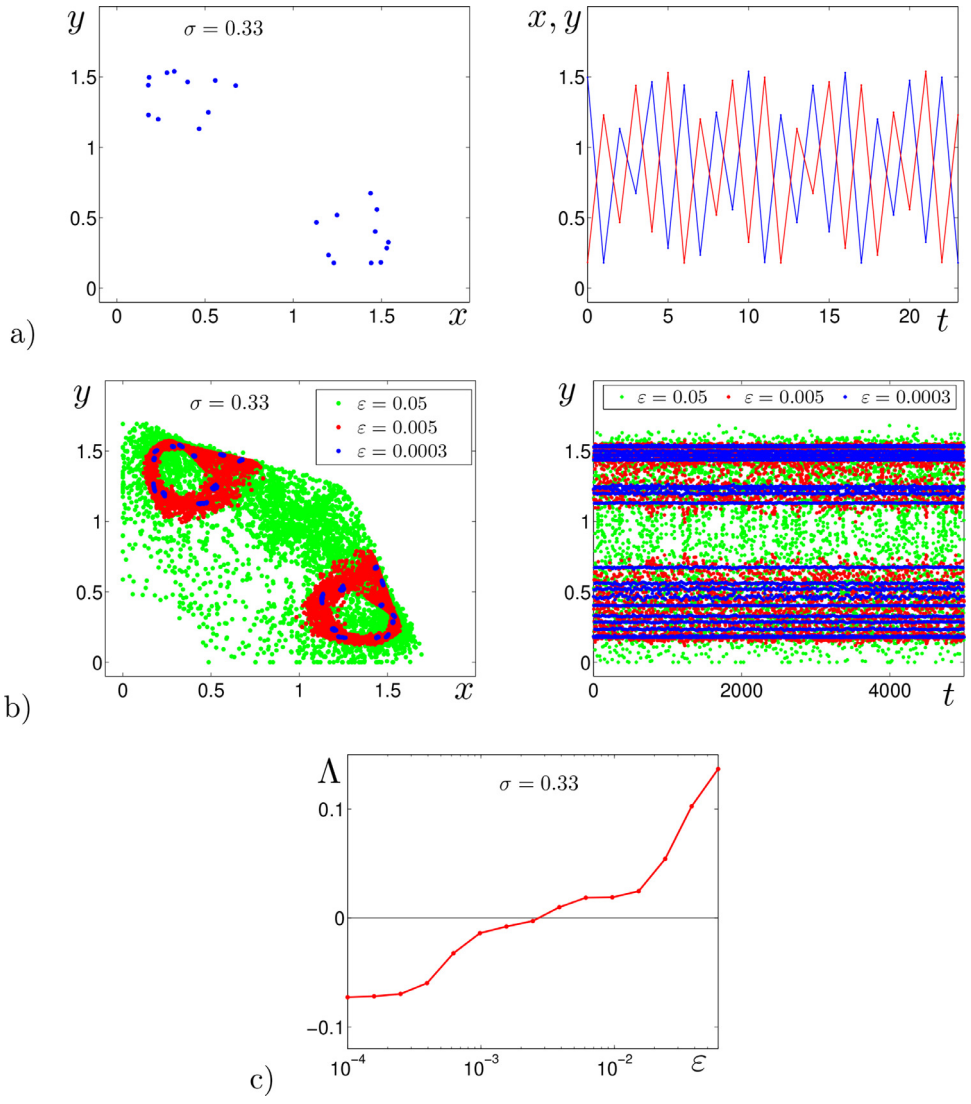

Fig. 8. Stochastic system (3) with $\sigma = 0.33$: a) states and corresponding time series for 22-cycle of the deterministic system; b) random states and time series for different values of the noise intensity; c) largest Lyapunov exponent Λ versus noise intensity ε.

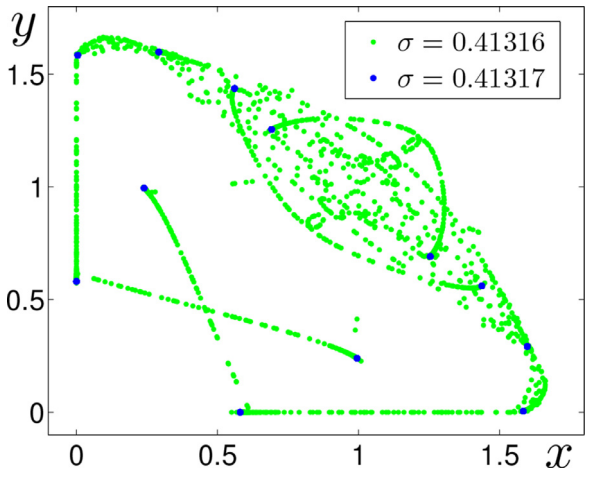

Fig. 9. Attractors of the deterministic system (1), (2) near the crisis bifurcation $\sigma_{cr} = 0.413163$: chaotic attractor (green) and 12-cycle (blue). (For interpretation of the references to color in this figure legend, the reader is referred to the web version of this article.)

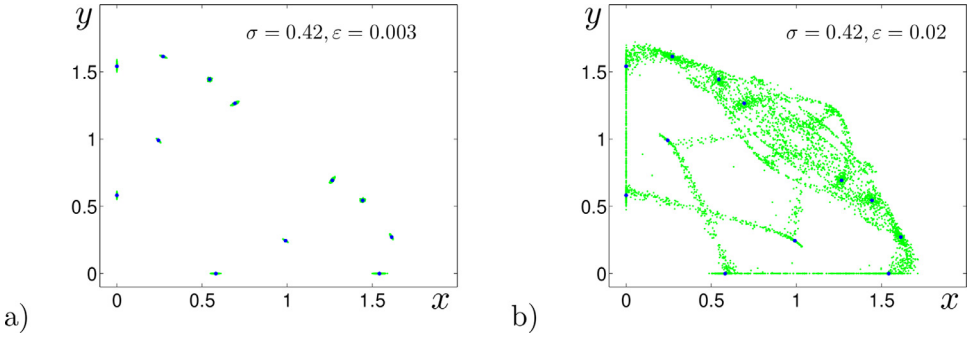

Fig. 10. Random states (green) of the stochastic system (3) with $\sigma = 0.42$ and a) $\varepsilon = 0.003$, b) $\varepsilon = 0.02$. States of the deterministic stable 12-cycle are plotted by blue points. (For interpretation of the references to color in this figure legend, the reader is referred to the web version of this article.)

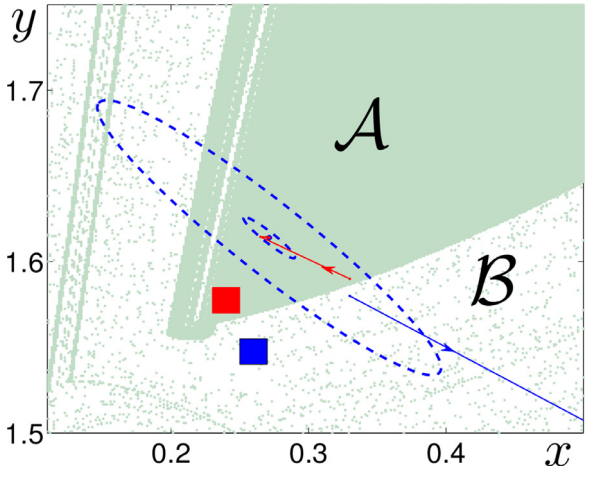

Fig. 11. Basin for $\mu = 1.8, \sigma = 0.42$ and confidence ellipses for $\varepsilon = 0.003$ and $\varepsilon = 0.02$. Fiducial probability $P = 0.99$.

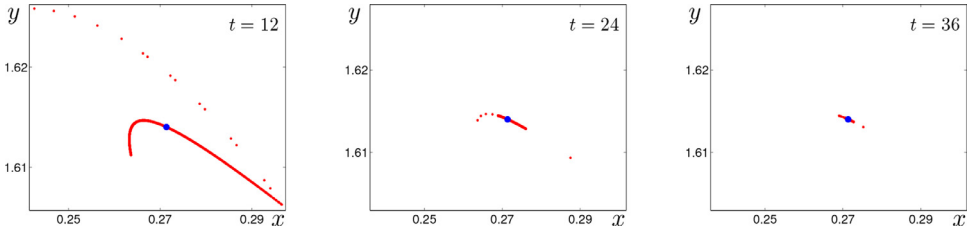

Fig. 12. States of the system with $\mu = 1.8, \sigma = 0.42$ starting at $t = 0$ from the nodes of the uniform grid on the red square $[0.23, 0.25] \times [1.57, 1.585]$. (For interpretation of the references to color in this figure legend, the reader is referred to the web version of this article.)

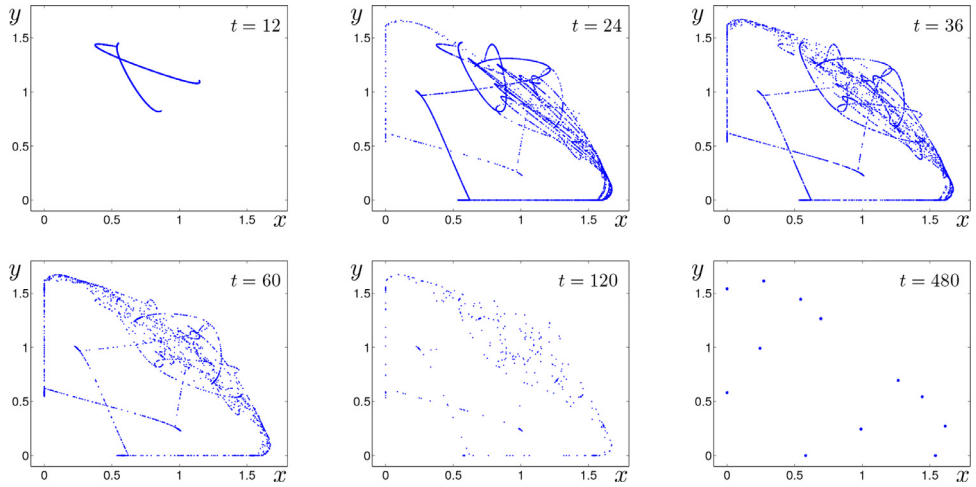

Fig. 13. States of the system with $\mu = 1.8, \sigma = 0.42$ starting at $t = 0$ from the nodes of the uniform grid on the blue square $[0.25, 0.27] \times [1.54, 1.555]$.

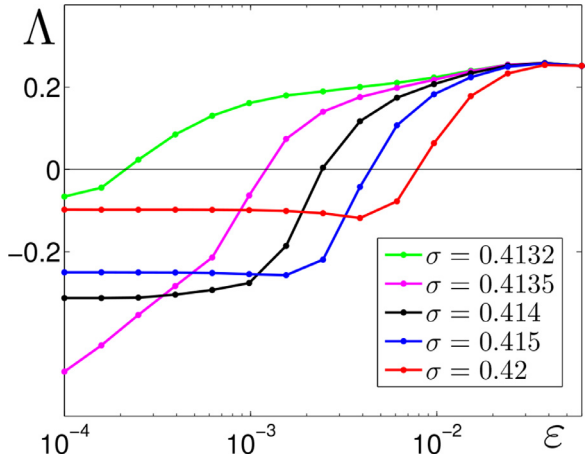

Fig. 14. Largest Lyapunov exponent for the stochastic system versus noise intensity ε.

Conclusion

In our paper, we studied transformations of the dynamical regimes in the metapopulation under variation of the intensity of migration and random disturbances. As a mathematical model, we used two coupled Ricker maps in the equilibrium mode. It was shown how under increasing coupling the initial deterministic model exhibits a rich variety of dynamical regimes, both regular and chaotic. It was revealed that under random forcing, the system demonstrates the following stochastic phenomena: (i) noise-induced destruction of anti-phase synchronization, (ii) temporal stabilization of the unstable equilibrium, (iii) transitions from order to chaos. To analyze these phenomena parametrically, we used statistics extracted from the direct numerical simulation, and the theoretical approach based on the stochastic sensitivity function technique. In this analysis, it was shown that chaotic transients and fractal riddled basins play a special role. It is worth noting that this approach can be utilized for the analysis of more complicated metapopulations.

Declaration of Competing Interest

The authors declare that they have no known competing financial interests or personal relationships that could have appeared to influence the work reported in this paper.

Acknowledgements

The study of the initial deterministic model (Sec.2) was supported by the Ministry of Science and Higher Education of the Russian Federation (Ural Mathematical Center project No. 075-02-2021-1387). The work on the investigation of stochastic phenomena and elaboration of theoretical methods of probabilistic analysis (Sec.3) was supported by the Russian Science Foundation (grant number 21-11-00062).

References

[1] Pikovski A, Rosenblum M, Kurths J. Synchronization: a universal concept in nonlinear sciences. Cambridge: Cambridge University Press; 2001.
[2] Boccaletti S, Pisarchik AN, del Genio CI, Amann A. Synchronization: from coupled systems to complex networks. Cambridge Univ Press; 2018.
[3] Rybalova EV, Strelkova GI, Anishchenko VS. Impact of sparse inter-layer coupling on the dynamics of a heterogeneous multilayer network of chaotic maps. Chaos Solitons Fractals 2021;142:110477. doi:10.1016/j.chaos.2020.110477.
[4] Pilosof S, Porter MA, Pascual M, Kéfi S. The multilayer nature of ecological networks. Nat Ecol Evol 2017;1:0101. doi:10.1038/s41559-017-0101.
[5] Demirel G, E B, Gross T. Dynamics of epidemic diseases on a growing adaptive network. Sci Rep 2017;7:42352. doi:10.1038/srep42352.
[6] Meunier D, Lambiotte R, Bullmore E. Modular and hierarchically modular organization of brain networks. Front Neurosci 2010;4:200. doi:10.3389/fnins.2010.00200.
[7] Hellmann F, Schultz P, Jaros P, Levchenko R, Kapitaniak T, Kurths J, et al. Network-induced multistability through lossy coupling and exotic solitary states. Nat Commun 2020;11:592. doi:10.1038/s41467-020-14417-7.
[8] Starnini M, Baronchelli A, Pastor-Satorras R. Effects of temporal correlations in social multiplex networks. Sci Rep 2017;7:8597. doi:10.1038/s41598-017-07591-0.
[9] Hogg T, Huberman BA. Generic behavior of coupled oscillators. Phys Rev A 1984;29:275–81. doi:10.1103/PhysRevA.29.275.
[10] Maistrenko YL, Maistrenko VL, Popovich A, Mosekilde E. Transverse instability and riddled basins in a system of two coupled logistic maps. Phys Rev E 1998;57:2713–24. doi:10.1103/PhysRevE.57.2713.
[11] Amritkar RE, Jalan S. Self-organized and driven phase synchronization in coupled map networks. Physica A 2003;321(1):220–5. doi:10.1016/S0378-4371(02)01750-8.
[12] Tanaka G, Sanjuán MAF, Aihara K. Crisis-induced intermittency in two coupled chaotic maps: towards understanding chaotic itinerancy. Phys Rev E 2005;71:016219. doi:10.1103/PhysRevE.71.016219.
[13] Zhusubaliyev ZT, Mosekilde E. Multilayered tori in a system of two coupled logistic maps. Phys Lett A 2009;373(10):946–51. doi:10.1016/j.physleta.2009.01.014.
[14] Bashkirtseva I, Ryashko L. Stochastic deformations of coupling-induced oscillatory regimes in a system of two logistic maps. Physica D 2020;411. doi:10.1016/j.physd.2020.132589.
[15] Savi MA. Effects of randomness on chaos and order of coupled logistic maps. Phys Lett A 2007;364(5):389–95. doi:10.1016/j.physleta.2006.11.095.
[16] Buscarino A, Gambuzza LV, Porfiri M, Fortuna L, Frasca M. Robustness to noise in synchronization of complex networks. Sci Rep 2013;3:2026. doi:10.1038/srep02026.

[17] Andreev AV, Makarov VV, Runnova AE, Pisarchik AN, Hramov AE. Coherence resonance in stimulated neuronal network. Chaos Solitons Fractals 2018;106:80–5. doi:10.1016/j.chaos.2017.11.017.
[18] Tyloo M, Delabays R, Jacquod P. Noise-induced desynchronization and stochastic escape from equilibrium in complex networks. Phys Rev E 2019;99:062213. doi:10.1103/PhysRevE.99.062213.
[19] Rybalova EV, Klyushina DY, Anishchenko VS, Strelkova GI. Impact of noise on the amplitude chimera lifetime in an ensemble of nonlocally coupled chaotic maps. Regul Chaotic Dyn 2019;24:432–45. doi:10.1038/s41598-017-07591-0.
[20] Bashkirtseva I, Ryashko L, Pisarchik AN. Stochastic transitions between in-phase and anti-phase synchronization in coupled map-based neural oscillators. Commun Nonlinear Sci NumerSimul 2021;95:105611. doi:10.1016/j.cnsns.2020.105611.
[21] Bashkirtseva I, Ryashko L. Chaotic transients, riddled basins, and stochastic transitions in coupled periodic logistic maps. Chaos 2021;31:053101. doi:10.1063/5.0050613.
[22] Hastings A. Complex interactions between dispersal and dynamics: Lessons from coupled logistic equations. Ecology 1993;74(5):1362–72. doi:10.2307/1940066.
[23] Aydogmus O. Phase transitions in a logistic metapopulation model with nonlocal interactions. Bull Math Biol 2018;80:228–53. doi:10.1007/s11538-017-0373-3.
[24] Kuperman MN, Laguna MF, Abramson G, Monjeau JA, Lanata JL. Metapopulation oscillations from satiation of predators. Physica A 2019;527:121288. doi:10.1016/j.physa.2019.121288.
[25] Lloyd AL. The coupled logistic map: a simple model for the effects of spatial heterogeneity on population dynamics. J Theor Biol 1995;173(3):217–30. doi:10.1006/jtbi.1995.0058.
[26] Kendall BE, Fox GA. Spatial structure, environmental heterogeneity, and population dynamics: Analysis of the coupled logistic map. Theor Popul Biol 1998;54(1):11–37. doi:10.1006/tpbi.1998.1365.
[27] Wysham DB, Hastings A. Sudden shifts in ecological systems: intermittency and transients in the coupled Ricker population model. Bull Math Biol 2008;70:1013–31. doi:10.1007/s11538-007-9288-8.
[28] Yakubu AA. Asynchronous and synchronous dispersals in spatially discrete population models. SIAM J Appl Dyn Syst 2008;7:284–310. doi:10.1137/070688122.
[29] Belyaev AV, Ryashko LB. Regular and chaotic regimes in the system of coupled populations. AIP Conf Proc 2020;2313:070023. doi:10.1063/5.0032976.
[30] Vortkamp I, Schreiber SJ, Hastings A, Hilker FM. Multiple attractors and long transients in spatially structured populations with an Allee effect. Bull Math Biol 2020;82:82. doi:10.1007/s11538-020-00750-x.
[31] Ricker WE. Stock and recruitment. J Fish Res Board Can 1954;11:559–623. doi:10.1139/f54-039.
[32] Alexander JC, Yorke JA, You Z, Kan I. Riddled basins. Int J Bifurcation Chaos 1992;02(04):795–813. doi:10.1142/S0218127492000446.
[33] Bashkirtseva I, Ryashko L, Tsvetkov I. Sensitivity analysis of stochastic equilibria and cycles for the discrete dynamic systems. Dyn Contin Discrete Impulsive Syst Ser A 2010;17:501–15.
[34] Bashkirtseva I, Ryashko L. Stochastic sensitivity of the closed invariant curves for discrete-time systems. Physica A 2014;410:236–43. doi:10.1016/j.physa.2014.05.037.
[35] Bashkirtseva I, Ryashko L. Stochastic sensitivity analysis of chaotic attractors in 2D non-invertible maps. Chaos Solitons Fractals 2019;126:78–84. doi:10.1016/j.chaos.2019.05.032.
[36] Ryashko LB, Bashkirtseva IA. On control of stochastic sensitivity. Autom Remote Control 2008;69:1171–80.
[37] Ryashko L, Slepukhina E. Noise-induced torus bursting in the stochastic Hindmarsh-Rose neuron model. Phys Rev E 2017;96:032212. doi:10.1103/PhysRevE.96.032212.
[38] Ryashko L. Sensitivity analysis of the noise-induced oscillatory multistability in Higgins model of glycolysis. Chaos 2018;28(3):033602. doi:10.1063/1.4989982.
[39] Belyaev A, Ryazanova T. Stochastic sensitivity of attractors for a piecewise smooth neuron model. J Differ Equ Appl 2019;25:1468–87. doi:10.1080/10236198.2019.1678596.